Journal of Energy Chemistry 56 (2021) 444–448

Contents lists available at ScienceDirect

Journal of Energy Chemistry

journal homepage: www.elsevier.com/locate/jechem

http://www.journals.elsevier.com/journal-of-energy-chemistry/

Letter

# Valence state of transition metal center as an activity descriptor for $CO_2$ reduction on single atom catalysts

Shisheng Zheng, Changjian Zuo, Xianhui Liang, Shunning Li *, Feng Pan *

*School of Advanced Materials, Peking University, Shenzhen Graduate School, Shenzhen 518055, Guangdong, China*

ARTICLE INFO

*Article history:*
Received 19 July 2020
Revised 19 August 2020
Accepted 20 August 2020
Available online 27 August 2020

*Keywords:*
$CO_2$ conversion
MXene based single-atom catalysts
Activity descriptor
Volcano shape relationship
First principles calculation

ABSTRACT



Carbon dioxide ($CO_2$) catalytic reduction has been passionately pursued for a long period of time due to its special importance in alleviating the greenhouse effect as well as generating valuable fuels and chemicals [1]. Among the various approaches for achieving $CO_2$ conversion, considerable efforts have been devoted to electrochemical reduction of $CO_2$ since this technology operates at ambient and mild environments and can potentially produce various useful products [2]. By now, a variety of electrocatalysts based on transition metals, transition metal oxides, and transition metal dichalcogenides [3–5], have been proposed for electrochemical $CO_2$ reduction reaction (CRR). Unfortunately, the current electrocatalysts are still confronted with two severe bottlenecks: Poor selectivity toward various products in CRR process, and the competition with hydrogen evolution reaction (HER) towards unwanted side-products [6]. The former originates from associated multielectron transfer process of CRR [7], while the latter is mainly due to the fact that the equilibrium potentials for most products of the CRR are very close to HER [8]. Thus, developing highly active and selective catalysts for electrochemical CRR remains one of the challenging issues in this field.

Recently, single-atom catalysts (SACs), where the isolated transition-metal (TM) atoms dispersed on perfect or defective surfaces serve as the active centers, have been widely investigated due to their superior catalytic performance along with a reduction in the amount of loaded precious metals. The high activity and selectivity can be ascribed to the unique electronic structure of isolated atoms, which is different from their bulk counterparts. SACs have already been investigated in a range of electrocatalysis processes, including oxygen evolution reaction (OER), nitrogen reduction reaction (NRR) and CRR [9–12].

The activity of SACs is significantly affected by the substrate environments. The ideal substrate should be able to anchor single atoms and possess outstanding stability and conductivity. Recently, a family of two-dimensional transition-metal carbides and nitrides ($M_{n+1}X_n$), known as MXene, were discovered and synthesized in experiments [13]. In the formula, "M" represents early transition metals, X corresponds to C or/and N, and $n$ = 1, 2 or 3. Owing to their high electronic conductivity, large surface areas, and tunable surface composition [14,15], MXenes are experimentally and theoretically proved to be promising candidates for binding metal atoms and for use as catalysts [16–21]. The basal planes of MXenes are usually terminated by functional groups (−OH, −F, and –O) after hydrogen fluoride treatment during their synthesis [13]. Nevertheless, recent studies have confirmed the possible elimination of –F group [13,22] and the –OH groups can be converted into –O groups after high-temperature annealing [23]. Therefor –O terminations are more representative of the real surface. In this work, we have theoretically investigated the potential of single transition metal (TM = Ti, V, Cr, Mn, Fe, Co, Ni, Cu, Zr, Nb,

* Corresponding authors.
*E-mail addresses:* lisn@pku.edu.cn (S. Li), panfeng@pkusz.edu.cn (F. Pan).

https://doi.org/10.1016/j.jechem.2020.08.023

Mo, Ru, Rh, Pd, Ag, Hf, Ta, W, Os, Ir, Pt, Au) atoms decorated on $Ti_2CO_2$, a typical MXene [24], as electrochemical catalysts for CRR (calculation details can be found in the Supporting Information). Our computational results demonstrate that Mn@$Ti_2CO_2$, Co@$Ti_2CO_2$ and Ni@$Ti_2CO_2$ are ideal candidates for electrochemical $CO_2$ reduction to $CH_4$, $CH_3OH$ and HCOOH, respectively. More importantly, we found that TM-to-substrate electron donation, as varied with different TM atoms, can be used as a simple descriptor to predict catalytic activity of TM@$Ti_2CO_2$ towards different CRR products. This work offers new insights to the design of high-efficiency MXene-based SACs for artificial $CO_2$ reduction.

To maintain the stability of TM@$Ti_2CO_2$ SACs for practical application, strong binding of TM atoms with $Ti_2CO_2$ is a prerequisite to prevent aggregation and detachment of the TM atoms. Therefore, we first investigate the geometry and thermodynamic stability of TM@$Ti_2CO_2$. As presented in Fig. 1(a and b), two possible binding sites were considered: (i) The hollow site between three neighboring O atoms and on the top site of C atom (Site 1), (ii) the hollow site between three neighboring O atoms and on the top site of Ti atom (Site 2). As shown in the upper panel of Fig. 1(c) and Table S1, most of the TM atoms tend to bind on the Site 1, and the value of binding energies between all the TM atoms and $Ti_2CO_2$ are positive, indicating a thermodynamic preference for TM atoms to be bonded to the substrate. To further investigate the kinetic stability of the TM atoms, we calculate the diffusion energy barriers of these TM atoms from the most stable site to the nearest second-stable site (Figs. S1, S2 and the lower panel of Fig. 1(c)). Previous studies demonstrated that, for the $CeO_2$ (1 1 1) surface, the Pd, Au and Pt atoms can rapidly diffuse with energy barriers of 0.14, 0.26, and 0.15 eV, respectively [25–27]. Given the similar surface structure of $CeO_2$ (1 1 1) and $Ti_2CO_2$ (both terminated by O atoms), we take $CeO_2$ (1 1 1) as a standard and select 0.3 eV as the threshold value to evaluate the kinetic stability of the TM atoms. As can be seen, the diffusion energy barriers of Cu, Pd, Ag, Pt and Au are less than 0.3 eV, indicating that they may easily diffuse on the surface and aggregate into clusters. Moreover, we find that the binding energies of these TM atoms are also relatively lower than other TM atoms, which further highlights their instability. Therefore, the Cu, Pd, Ag, Pt and Au decorated $Ti_2CO_2$ are considered to be unstable and excluded for further investigation.

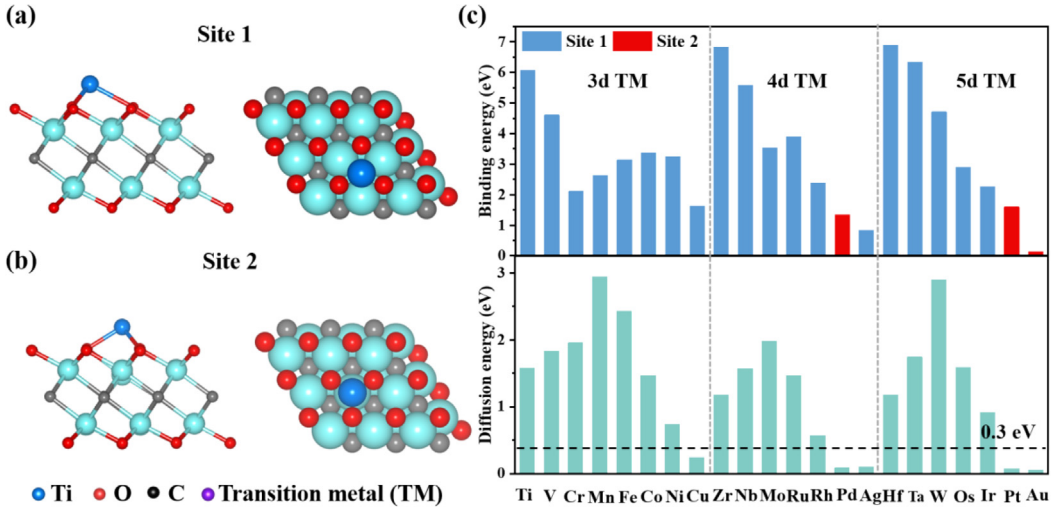


**Fig. 1.** The two possible adsorption sites, (a) site 1 and (b) site 2, of TM atoms on $Ti_2CO_2$. (c) The binding energies and the diffusion energy barriers for different TM atoms on $Ti_2CO_2$. For each SAC, only the binding energy of the most stable adsorption configuration is given, and the diffusion pathway goes from the most stable site to the nearest second stable site.

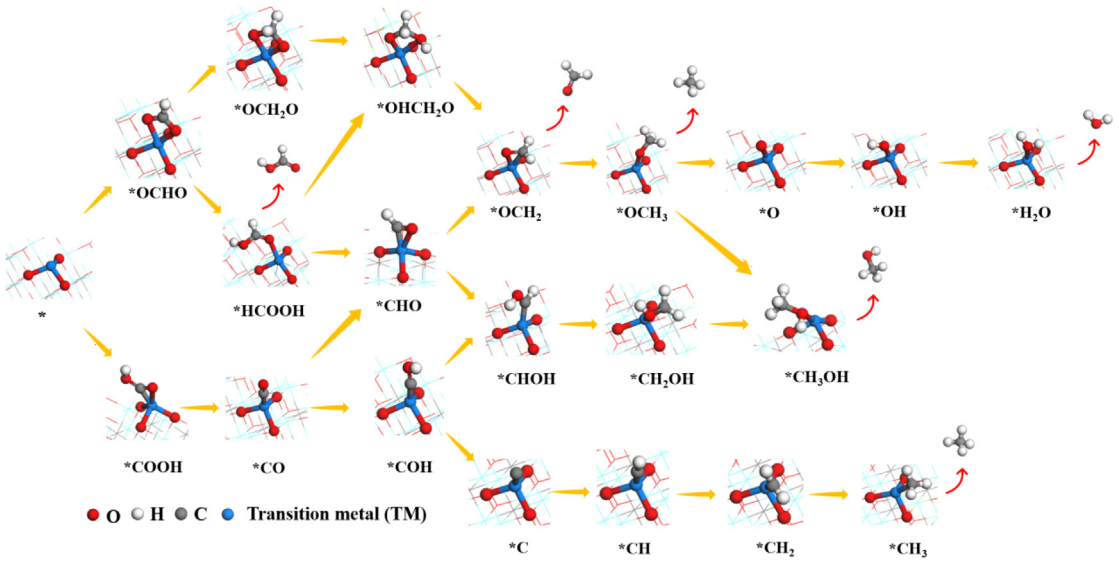


**Fig. 2.** Schematic of mechanisms for $CO_2$ reduction to different C1 products.

Using the most stable TM@$Ti_2CO_2$ geometries, we then examined the CRR catalytic performance of TM@ $Ti_2CO_2$. $CO_2$ reduction to C1 products can proceed through different reactions that involve 2–8 electrons (Fig. 2). Particularly, due to the lack of TM ensembles in TM@$Ti_2CO_2$ for C–C coupling, the pathways to C2 products were not examined [28,29].

The CRR begins with the hydrogenation of $CO_2$ to form either carboxyl (*COOH) or formate (*HCOO) on the active center (Fig. 2), while in this process, the HER process may also consume the protons and electrons under the same reaction condition, occupying the active center and resulting in a low selectivity and Faradic efficiency. It is generally believed that the free energy change of initial protonation step for CRR ($CO_2 + H^+ + e^- \rightarrow$ *HCOO/*COOH) and HER ($H^+ + e^- \rightarrow$ *H) can be investigated to evaluate the selectivity [28,30]. The results are summarized in Fig. 3(a), it is found that the reaction of *HCOO formation is energetically more favorable than the *COOH formation on all TM@$Ti_2CO_2$ and the difference in $\Delta G$ between them is greater than 0.3 eV in most cases (see Table S2), indicating a high preference towards the *HCOO pathway on the TM@$Ti_2CO_2$. Therefore the *COOH reduction pathways were not further investigated and the CO product, which can only be hydrogenated from *COOH intermediate, is expected not to be formed in the TM@$Ti_2CO_2$ system. For all the TM@$Ti_2CO_2$ SACs, the calculated values of free energy changes for ($H^+ + e^- \rightarrow$ *H) reaction are more positive than the first protonation step of CRR ($CO_2 + H^+ + e^- \rightarrow$ *HCOO), which indicates that the TM catalytic center on $Ti_2CO_2$ substrate can effectively promote CRR over HER.

We further consider the protonation of *HCOO intermediate. As shown in Fig. 2, the second protons can attack the C or O atom of *HCOO, generating *HCOOH or *$H_2COO$ intermediates. In the former case, formic acid can be formed after the direct desorption of the intermediate. The further hydrogenation of *HCOOH or *$H_2COO$ would lead to the four-electron product of $OCH_2$. Nevertheless, it is unlikely to be the final product because its binding strength is relatively strong on all the TM@$Ti_2CO_2$ SACs (>1 eV, see Fig. S10), which indicates that *$OCH_2$ can serve as key intermediates for further protonation to six-electron product ($CH_3OH$) or eight-electron product ($CH_4$).

The reaction pathway for each TM@$Ti_2CO_2$ is determined by the most energetically favorable intermediate at each hydrogenation step. After screening all the possible intermediates, the most energetically favorable product, the potential determining step (PDS) and the reaction free energy at PDS ($\Delta G_{PDS}$) for all TM@$Ti_2CO_2$ are summarized in Fig. 3(b). It is shown that TM@$Ti_2CO_2$ electrocatalysts can produce three kinds of C1 products, namely HCOOH, $CH_3OH$ and $CH_4$, demonstrating the essential role of TM catalytic center in determining the final CRR product.

For Ti, V, Cr, Mn, Zr, Nb, Mo, Ru, Hf, Ta, W, Os and Ir SACs, $CH_4$ is expected to be the final product. The Mn@$Ti_2CO_2$ exhibits the most promising catalytic activity with the following intermediates (Fig. 3(c)): $CO_2 \rightarrow$ *HCOO $\rightarrow$ *HCOOH $\rightarrow$ *$H_2COOH \rightarrow$ *$OCH_2 \rightarrow$ *$OCH_3 \rightarrow$ *O + $CH_4 \rightarrow$ *OH $\rightarrow H_2O$. The pathway is different from that on the Cu (1 1 1) surface and the *HCOO $\rightarrow$ *HCOOH is identified as the PDS with a $\Delta G_{PDS}$ of 0.59 eV, which is also well below that on the Cu (1 1 1) surface (0.99 eV) [31]. Intriguingly, for early transition metal SACs, the reaction pathways are uniform and the energy profiles show remarkable similarity (Fig. S4), which is probably due to their similar electronic structures. The last hydrogenation step (*OH + $H^+ + e^- \rightarrow H_2O$) is identified as the PDS with $\Delta G_{PDS}$ all greater than 1 eV (see Fig. S4), this rules out their potential to reduce $CO_2$ because the *OH would block the catalytic center and leads to the deactivation of the catalysts [31].

The Fe, Co and Rh SACs tend to generate $CH_3OH$ product. Co@$Ti_2CO_2$ shows the highest activity, following the pathway (Fig.3(d)): $CO_2 \rightarrow$ *HCOO $\rightarrow$ *HCOOH $\rightarrow$ *CHO $\rightarrow$ *$OCH_2 \rightarrow$ *$OCH_3 \rightarrow CH_3OH$. The PDS is the $CO_2 \rightarrow$ *HCOO step and the corresponding $\Delta G_{PDS}$ is as low as 0.28 eV, which is well below that on Cu (2 1 1) (0.74 eV) [7] surface and competitive to other theoretically studied $CO_2$ to $CH_3OH$ single atom catalysts, including V decorated $\beta_{12}$ boron monolayer (0.54 eV) [32], Ni decorated $C_2N$ monolayer (0.31 eV) [29] and Pt supported on defective graphene (0.27 eV) [28].

Ni@$Ti_2CO_2$ is the only catalysts that tend to produce HCOOH with the intermediates (Fig. 3(e)): $CO_2 \rightarrow$ *HCOO $\rightarrow$ HCOOH. The PDS is identified as the $CO_2 \rightarrow$ *HCOO step with a $\Delta G_{PDS}$ at 0.29 eV, which is also significantly lower than that on Cu (2 1 1) surface (0.48 eV) [33] and is competitive to the traditional catalysts for the formation of formic acid, such as the partially oxidized atomic Co layers (0.24 V) [34] and Pd nanoparticles (NPs) dispersed on a carbon support (0.20 V) [35].

It is beneficial to search an activity descriptor to establish a "volcano" relationship on catalytic behaviors such that we can further understand the superior catalytic activity of Mn@$Ti_2CO_2$, Co@$Ti_2CO_2$ and Ni@$Ti_2CO_2$ SACs. It is generally agreed that the electronic structures of catalytic centers would greatly influence the electron transfer and reaction energy in catalytic processes. Hereby, we first examined the descriptor of *d* band center, which

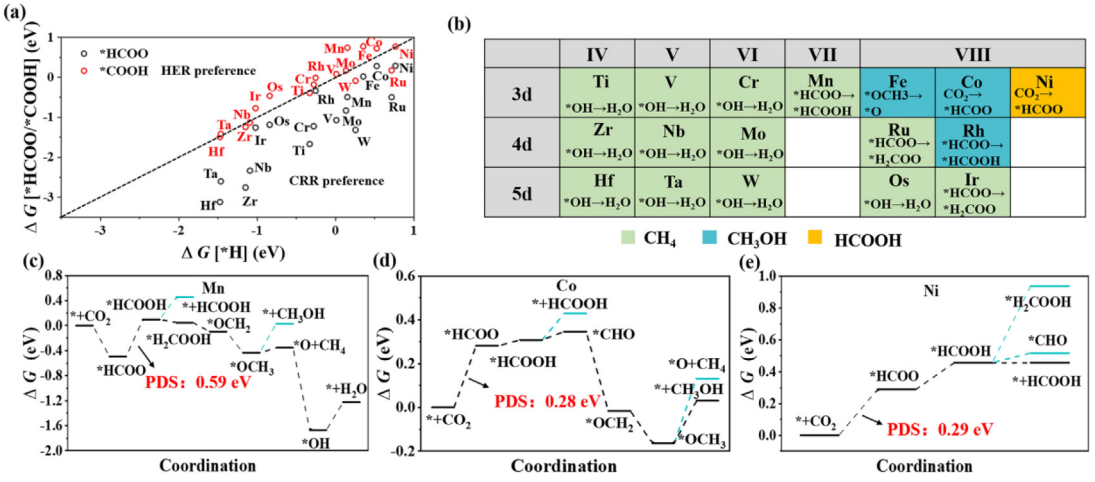


**Fig. 3.** (a) The reaction free energy change ($\Delta G$) of *HCOO and *COOH formation vs HER. (b) Summary of the most energetically favorable product, the potential determining step (PDS) and the reaction free energy at PDS ($\Delta G_{PDS}$) for each investigated TM@$Ti_2CO_2$. The free energy profiles for CRR catalyzed by (c) Mn@ $Ti_2CO_2$, (d) Co@ $Ti_2CO_2$, and (e) Ni@ $Ti_2CO_2$.

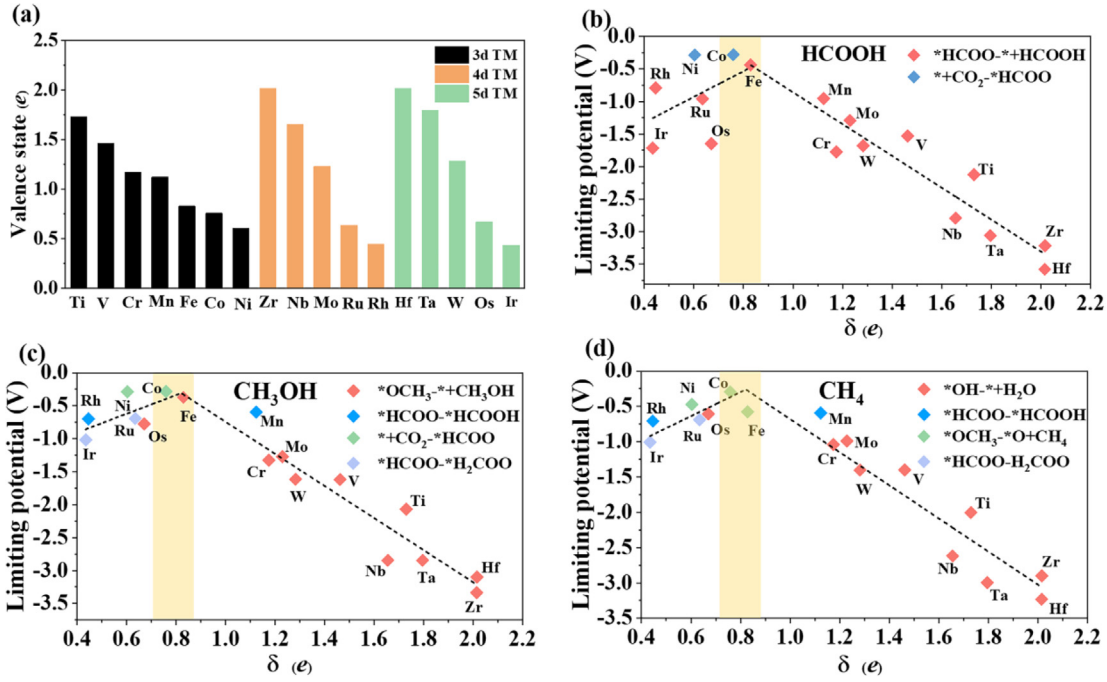


**Fig. 4.** (a) The valence states of TMs when they are decorated on $Ti_2CO_2$ substrate. The limiting potential towards (b) HCOOH, (c) $CH_3OH$ and (d) $CH_4$ as a function of the valence state of TM atoms. Different colored points correspond to different PDS.

can be used to explain the general catalytic activity trend for different catalytic processes, e.g. CRR, NRR, and ORR [36,37], in bulk metals. As presented in Fig. S9, there is not obvious relationship between the *d* band center of TM@$Ti_2CO_2$ and the limiting potential of the three different products, which can be attributed to a different electronic structure of the single TM atoms from that in the bulk.

Based on the above results and analysis, we inspect the charge redistribution of TM atoms when it is decorated on the $Ti_2CO_2$ substrate through Bader charge analysis [38]. We define the valence state of different TM atoms as the number of electrons transferred from the TM atom to the O atoms. As shown in Fig. 4(a), the valence state of different TM atoms varies in a range from ~0.4 e to ~2 e, indicating that the interplay between transition metal *d* orbitals and O *p* orbitals can effectively influence the valence state of the TM atoms, and in each period, a decreasing trend can be clearly observed.

Moreover, it is known that the TM atoms can provide both empty *d* orbitals to accept electrons to form a coordination bond and lone electrons to form a covalent bond [39]. Hence, the valence state of TMs would directly influence the bonding strength with the intermediates, which is substantiated by the calculated adsorption energies of all intermediates involved in our system, as shown in Fig. S10. For all intermediates, a volcano shape relationship can be roughly observed. It can be assumed that the valence state of TMs could be used as an activity descriptor, wherefore the limiting potential towards different products as a function of the valence state of TMs is shown in Fig. 4. A volcano trend is observed for each kind of product, with the optimal scope of valence state ranging from ~0.7 e to ~0.9 e. The Fe@$Ti_2CO_2$ and Co@$Ti_2CO_2$ locate within the above region for three cases, indicating that they are the most active catalysts for CRR and tend to generate $CH_3OH$ rather than $CH_4$ or HCOOH according to the reaction free energy profile. The volcano trend follows the Sabatier principle [40], which states that a promising catalyst should bind the intermediates neither too strong nor too weak. This simple descriptor well explains the catalytic performance of the TM@$Ti_2CO_2$ SACs, and suggest that a certain moderate degree of electron transference from TM atoms to the substrate will be expected to promote the overall catalytic activity.

In summary, we performed DFT calculations to evaluate the potential of single TM atom decorated $Ti_2CO_2$ for the electrochemical reduction of $CO_2$ and discovered a simple descriptor that can reliably describe the catalytic performance of TM@$Ti_2CO_2$. Mn@$Ti_2CO_2$ tends to produce $CH_4$ with limiting potential lower than that of Cu (1 1 1) surface. Co@$Ti_2CO_2$ is revealed as an excellent electrocatalyst for $CH_3OH$ production with limiting potential at −0.28 V, competitive to the most active electrocatalysts found in previous reports. Ni@$Ti_2CO_2$ is revealed to be a superior catalyst to produce HCOOH with limiting potential value calculated to be −0.29 V, which is well below that of Cu (2 1 1) surface. It is found that the valence state of TM atoms can effectively affect the binding strength of intermediates and is therefore proposed as a descriptor for the catalytic activity in CRR. Hereby, a volcano shaped relationship between the descriptor and the catalytic activity is demonstrated and a certain moderate degree (around 0.8 e) of TM-to-substrate electron donation would be beneficial for effective $CO_2$ reduction. It is expected that this simple descriptor would enrich the design principles for guiding the rational design of MXene based single atom catalysts for boarder application.

## Declaration of Competing Interest

The authors declare that they have no known competing financial interests or personal relationships that could have appeared to influence the work reported in this paper.

## Acknowledgments

This work was supported by Soft Science Research Project of Guangdong Province (No. 2017B030301013) and Shenzhen Science and Technology Research Grant (ZDSYS201707281026184).

## Appendix A. Supplementary data

Supplementary data to this article can be found online at https://doi.org/10.1016/j.jechem.2020.08.023.

## References

[1] G.A. Olah, G.K. Prakash, A. Goeppert, J. Am. Chem. Soc. 133 (2011) 12881–12898.
[2] D.T. Whipple, P.J.A. Kenis, J. Phys. Chem. Lett. 1 (2010) 3451–3458.
[3] J. Wu, Y. Huang, W. Ye, Y. Li, Adv. Sci. 4 (2017) 1700194.
[4] W. Zhang, Y. Hu, L. Ma, G. Zhu, Y. Wang, X. Xue, R. Chen, S. Yang, Z. Jin, Adv. Sci. 5 (2018) 1700275.
[5] K. Ye, G.X. Wang, X.H. Bao, Chinese. J. Struc. Chem. 39 (2020) 206–213.
[6] A. Vasileff, Y. Zheng, S.Z. Qiao, Adv. Energy Mater. 7 (2017) 1700759.
[7] A.A. Peterson, F. Abild-Pedersen, F. Studt, J. Rossmeisl, J.K. Norskov, Energy Environ. Sci. 3 (2010) 1311–1315.
[8] R. Kortlever, J. Shen, K.J. Schouten, F. Calle-Vallejo, M.T. Koper, J. Phys. Chem. Lett. 6 (2015) 4073–4082.
[9] Y. Peng, B. Lu, S. Chen, Adv. Mater. 30 (2018) e1801995.
[10] B.K. Zhang, Z.Z. Li, Q. Li, Z. Lin, J. Liu, F. Pan, Chinese J. Struc. Chem. 39 (2020) 189–199.
[11] M. Qiu, H.L. Tao, Y. Li, X. Huang, Y.F. Zhang, Chinese J. Struc. Chem. 37 (2018) 665–678.
[12] D. Liu, Q. He, S. Ding, L. Song, Adv. Energy Mater. (2020) 2001482.
[13] M. Naguib, M. Kurtoglu, V. Presser, J. Lu, J. Niu, M. Heon, L. Hultman, Y. Gogotsi, M.W. Barsoum, Adv. Mater. 23 (2011) 4248–4253.
[14] M. Naguib, O. Mashtalir, J. Carle, V. Presser, J. Lu, L. Hultman, Y. Gogotsi, M.W. Barsoum, ACS Nano 6 (2012) 1322–1331.
[15] B. Anasori, M.R. Lukatskaya, Y. Gogotsi, Nat. Rev. Mater. 2 (2017) 16098.
[16] B. Huang, N. Li, W.-J. Ong, N. Zhou, J. Mater. Chem. A 7 (2019) 27620–27631.
[17] S. Zheng, S. Li, Z. Mei, Z. Hu, M. Chu, J. Liu, X. Chen, F. Pan, J. Phys. Chem. Lett. 10 (2019) 6984–6989.
[18] R.P. Pandey, K. Rasool, V.E. Madhavan, B. Aïssa, Y. Gogotsi, K.A. Mahmoud, J. Mater. Chem. A 6 (2018) 3522–3533.
[19] X. Zhang, Y. Zhang, C. Cheng, Z. Yang, K. Hermansson, Nanoscale 12 (2020) 12497–12507.
[20] A. Liu, X. Liang, X. Ren, W. Guan, M. Gao, Y. Yang, Q. Yang, L. Gao, Y. Li, T. Ma, Adv. Funct. Mater. (2020) 2003437.
[21] L.X. Zhang, X.Y. Pan, G.T. Wang, X. Long, Z.G. Yi, Chinese J. Struc. Chem. 37 (2018) 1457–1469.
[22] X.-H. Zha, K. Luo, Q. Li, Q. Huang, J. He, X. Wen, S. Du, EPL 111 (2015) 26007.
[23] Y. Xie, M. Naguib, V.N. Mochalin, M.W. Barsoum, Y. Gogotsi, X. Yu, K.W. Nam, X.Q. Yang, A.I. Kolesnikov, P.R. Kent, J. Am. Chem. Soc. 136 (2014) 6385–6394.
[24] M. Naguib, V.N. Mochalin, M.W. Barsoum, Y. Gogotsi, Adv. Mater. 26 (2014) 992–1005.
[25] Y.Q. Su, J.X. Liu, I.A.W. Filot, E.J.M. Hensen, Chem. Mater. 29 (2017) 9456–9462.
[26] K.M.N. Albert Bruix, Francesc Illas, J. Phys. Chem. C 122 (34) (2018) 19712–19721, 114 (2010) 14202–14207.
[27] Y.G. Wang, D. Mei, V.A. Glezakou, J. Li, R. Rousseau, Nat. Commun. 6 (2015) 6511.
[28] S. Back, J. Lim, N.Y. Kim, Y.H. Kim, Y. Jung, Chem. Sci. 8 (2017) 1090–1096.
[29] X. Cui, W. An, X. Liu, H. Wang, Y. Men, J. Wang, Nanoscale 10 (2018) 15262–15272.
[30] Z. Zhao, G. Lu, ACS Catal. 8 (2018) 3885–3894.
[31] Y. Li, H. Su, S.H. Chan, Q. Sun, ACS Catal. 5 (2015) 6658–6664.
[32] C. Ling, Q. Li, A. Du, J. Wang, ACS Appl. Mater. Interfaces 10 (2018) 36866–36872.
[33] Y. Feng, W. An, Z. Wang, Y. Wang, Y. Men, Y. Du, ACS Sustainable Chem. Eng. 1 (2019) 210–222.
[34] S. Gao, Y. Lin, X. Jiao, Y. Sun, Q. Luo, W. Zhang, D. Li, J. Yang, Y. Xie, Nature 529 (2016) 68–71.
[35] X. Min, M.W. Kanan, J. Am. Chem. Soc. 137 (2015) 4701–4708.
[36] F.H.B. Lima, J. Zhang, M.H. Shao, K. Sasaki, M.B. Vukmirovic, E.A. Ticianelli, R.R. Adzic, J. Phys. Chem. C 111 (2007) 404–410.
[37] F. Abild-Pedersen, J. Greeley, F. Studt, J. Rossmeisl, T.R. Munter, P.G. Moses, E. Skulason, T. Bligaard, J.K. Norskov, Phys. Rev. Lett. 99 (2007) 016105.
[38] W. Tang, E. Sanville, G. Henkelman, J. Phys. Condens. Matter 21 (2009) 084204.
[39] L. Gong, D. Zhang, C.Y. Lin, Y. Zhu, Y. Shen, J. Zhang, X. Han, L. Zhang, Z. Xia, Adv. Energy Mater. 9 (2019) 1902625.
[40] A.J. Medford, A. Vojvodic, J.S. Hummelshøj, J. Voss, F. Abild-Pedersen, F. Studt, T. Bligaard, A. Nilsson, J.K. Nørskov, J. Catal. 328 (2015) 36–42.